JACS
JOURNAL OF THE AMERICAN CHEMICAL SOCIETY
Communication
pubs.acs.org/JACS

Designing a Deep-Ultraviolet Nonlinear Optical Material with a Large Second Harmonic Generation Response

Hongping Wu,[†] Hongwei Yu,[†] Zhihua Yang,[†] Xueling Hou,[†] Xin Su,[†] Shilie Pan,*[,†] Kenneth R. Poeppelmeier,[‡] and James M. Rondinelli*[,§]

[†]Xinjiang Key Laboratory of Electronic Information Materials and Devices, Xinjiang Technical Institute of Physics & Chemistry, Chinese Academy of Sciences, Urumqi 830011, China

[‡]Department of Chemistry, Northwestern University, Evanston Illinois 60208-3131, United States

[§]Department of Materials Science and Engineering, Drexel University, Philadelphia, Pennsylvania 19104-2816, United States

Supporting Information

ABSTRACT: The generation of intense coherent deep-UV light from nonlinear optical materials is crucial to applications ranging from semiconductor photolithography and laser micromachining to photochemical synthesis. However, few materials with large second harmonic generation (SHG) and a short UV-cutoff edge are effective down to 200 nm. A notable exception is $KBe_2BO_3F_2$, which is obtained from a solid-state reaction of highly toxic beryllium oxide powders. We designed and synthesized a benign polar material, $Ba_4B_{11}O_{20}F$, that satisfies these requirements and exhibits the largest SHG response in known borates containing neither lone-pair-active anions nor second-order Jahn–Teller-active transition metals. We developed a microscopic model to explain the enhancement, which is unexpected on the basis of conventional anionic group theory arguments. Crystal engineering of atomic displacements along the polar axis, which are difficult to attribute to or identify within unique anionic moieties, and greater cation polarizabilities are critical to the design of next-generation SHG materials.

Nonlinear optical (NLO) materials that are able to halve the wavelength of light (or double the frequency) rely on the process of second harmonic generation (SHG),[1] which occurs only when inversion symmetry is absent in a crystal. The availability of SHG materials operating in the deep-UV region[2] is limited by fundamental requirements imposed on the crystalline structure: they should exhibit a large NLO response while also possessing a broad UV transparency window and phase matching. Finding an optimal composition that is easy to synthesize, yields large single crystals, and satisfies the NLO requirements is a serious materials discovery challenge.

Commonly, NLO materials with large SHG response are constructed by incorporating acentric structural units with a nonvanishing hyperpolarizability, such as second-order Jahn–Teller (SOJT) polar displacements of d^0 metal centers (Ti^{4+}, Ta^{5+}, Mo^{6+}, etc.),[3] stereochemically lone-pair-active anions (LPAAs) ($[IO_3]^-$, $[TeO_x]^{n-}$, etc.),[4] or polar chalcogenide units ($[AsS_3]^{3-}$, $[SbS_3]^{3-}$, $[TeS_3]^{2-}$).[5,6] While these structural units lead to large NLO responses, they also produce an unwanted shift in the UV absorption edge to longer λ, making them less suitable for deep-UV applications. To circumvent this problem, basic structural units with excitation energies near the UV are necessary. One such unit, $[B_3O_6]^{3-}$, is found in β-BaB_2O_4 (BBO),[7] which is transparent down to 190 nm and shows significant SHG. However, BBO cannot achieve the desired deep-UV response using $[B_3O_6]^{3-}$ units alone.

Here we describe a design strategy to realize a deep-UV material with a large SHG response by the introduction of fluorine into BBO. Our approach relies on an early observation[8] that established a proportionality between the macroscopic NLO response and spontaneous polarization owing to lifting of the inversion symmetry by atomic displacements within a unit cell. Leveraging that insight, we synthesized $Ba_4B_{11}O_{20}F$ (BBOF) with a polar structure that is far from centrosymmetric, yielding an SHG response at 1064 nm exceeding that of KH_2PO_4 (KDP) by nearly an order of magnitude. Surprisingly, conventional anionic group theory[9] indicates that the SHG response of BBOF should be lower than that of BBO. We show that a crystallographic-based polar displacement analysis,[10] which captures the degree to which inversion symmetry is absent, is needed to understand the SHG enhancement. Our model discriminates polar atomic displacements from the ambiguous acentric distortions of B_xO_y polyhedral units. F-atom-directed cooperative polar displacements and an enhanced Ba cation polarizability, evaluated using density functional theory (DFT), are captured within our framework. The linkage of B–O groups in BBOF eliminates the terminal O atoms, making BBOF transparent to 175 nm, suitable for deep-UV applications.

Motivated by the deep-UV NLO material $KBe_2BO_3F_2$ and the structure-directing capabilities of oxyfluoride anionic groups,[11] we synthesized BBOF by solid-state reaction techniques as described in the Supporting Information (SI). The phase purity was confirmed by powder X-ray diffraction (PXRD) (Figure S1), and the polar $Cmc2_1$ structure was determined by single-crystal XRD (see the SI; Table S1 lists the crystal data and structure refinement details). The UV–vis–IR diffuse-reflectance spectrum showed that the F atoms shifted the UV absorption edge[11a] into the deep-UV region at ~175 nm (Figure S3). Differential scanning calorimetry and thermogravimetric analyses showed that BBOF melts incongruently (Figure S4), and PXRD on the

Received: January 16, 2013
Published: February 28, 2013

   dx.doi.org/10.1021/ja400500m | J. Am. Chem. Soc. 2013, 135, 4215–4218

resulting polycrystalline material confirmed it to be a mixture of β-BaB_2O_4 and an unidentified amorphous product.

BBOF has a complex framework structure (Figure 1a) formed from two main units. One is a new functional building block

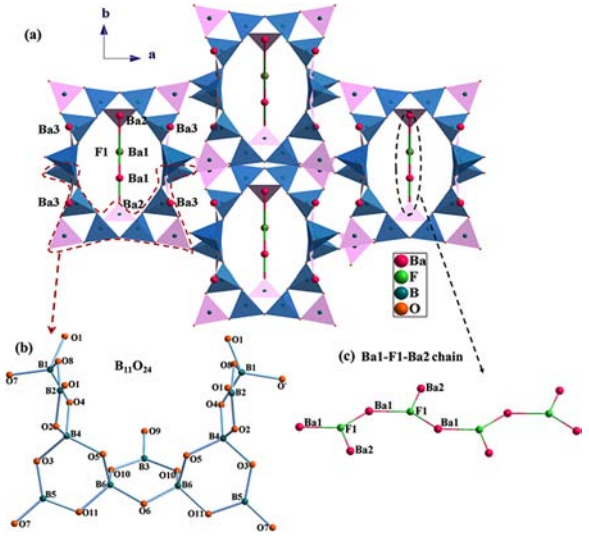

Figure 1. (a) View of the 3D framework of $Ba_4B_{11}O_{20}F$ along the *c* axis. Ba−O bonds have been omitted for clarity. BO_4 groups, light blue; BO_3 groups, pink. (b) $B_{11}O_{24}$ FBB. (c) Ba1−F1−Ba2 chain.

(FBB), $B_{11}O_{24}$, composed of five B_3O_8 rings connected by shared O atoms to give a three-dimensional (3D) network with tunnels along the *c* axis (Figure 1b). The B atoms within the FBB exhibit two coordination environments, BO_3 triangles and BO_4 tetrahedra (Figure S6). The other unit is Ba1−F1−Ba2 chains, which fill the tunnels formed by linking of the FBBs; Ba3 atoms are located in the periphery of the tunnels. In these chains, each F1 is shared by two Ba1 and one Ba2 (Figure 1c). There are three Ba coordination environments: F-sharing $Ba1O_5F_2$ and $Ba2O_7F$ polyhedra and $Ba3O_{10}$ units (Figure S7).

The FBB in BBOF and the borate network in BBO share structural commonalities. BBOF exhibits three- and four-coordinate borate units that link to form B_3O_8 rings, while BBO exclusively exhibits three-coordinate borate units that link to form B_3O_6 rings.[12] Unlike BBOF, the Ba atoms in BBO are found in two unique BaO_8 polyhedra. Figure 2 shows pair distribution functions (PDFs) for BBO and BBOF. The B−O distances in the BO_3 units are nearly the same in the two compounds. The trigonal [tetrahedral] B atoms in BBOF have B−O bond distances of 1.354(5)−1.373(5) Å [1.399(16)−1.510(4) Å] with an average distance of 1.368 Å [1.467 Å],

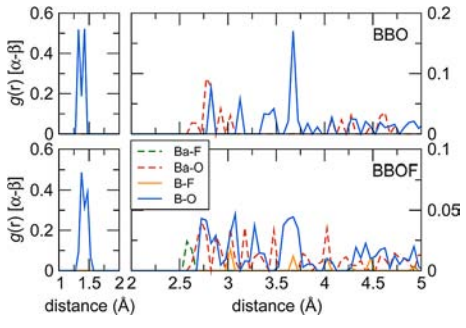

Figure 2. Atom-decomposed (α−β) PDFs for BBO and BBOF.

producing the two-peak feature in the PDF (Figure 2 left). The most distinctive structural difference is that the Ba−O bond distances of 2.619(3)−3.300(7) Å (av 2.807 Å) in BBOF are shorter than those in BBO. There is a shift in the number of Ba−O pairs having a distance of 1.6 Å toward 2.6 Å in going from BBO to BBOF, and slightly shorter Ba−F bond distances appear in a narrower interval [2.557(3)−2.632(3) Å], indicating that Ba−F interactions influence the atomic structure.

We measured the SHG response of BBOF by the Kurtz−Perry method[13] on sieved powder samples using a Q-switched Nd:YAG laser (1064 nm). BBOF exhibits a very large SHG response, ∼10 times that of KDP and ∼1.8 times that of BBO at the same particle size (0.3−0.4 mm) (Figure 3a). The intensity is the largest reported to date for a borate compound containing neither LPAAs nor SOJT-active transition metals, and BBOF is type-1 phase-matchable (Figure 3b).

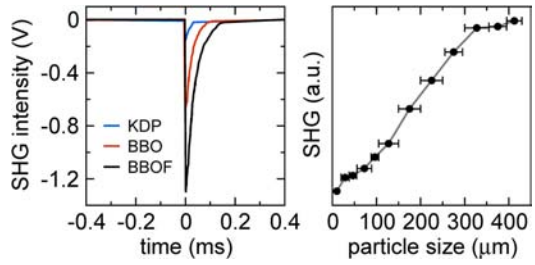

Figure 3. (left) Oscilloscope traces showing SHG intensities for BBOF and for KDP and BBO as references. (right) Phase-matching curve for BBOF. The solid curve is a guide for the eyes, not a fit to the data.

To determine the origin of the enhanced SHG response, we first applied anionic group theory,[9] which correlates the macroscopic SHG behavior to acentric distortions of the polyhedral building units and the collective alignment of their local dipoles.[14] We computed the direction and magnitude of the $Ba1O_5F_2$, $Ba2O_7F$, $Ba3O_{10}$, and $B_{11}O_{24}$ dipole moments using a bond-valence approach[15] and compared them with those of the three structural units in BBO (Table 1). The magnitude of the

Table 1. Components and Magnitudes (in Debye) of the Polyhedral Dipole Moments of BBOF and BBO

	species	*x* (*a*)	*y* (*b*)	*z* (*c*)	magnitude
BBOF	$Ba1O_5F_2$	0	7.37	1.95	7.62
	$Ba2O_7F$	0	−4.64	−2.84	5.44
	$Ba3O_{10}$	−0.58	2.33	0.31	2.42
	$B_{11}O_{24}$	0	−1.78	4.45	4.79
BBO	$Ba1O_8$	−0.9	−2.01	−1.3	2.17
	$Ba2O_8$	−0.8	−1.58	−1.58	2.09
	B_3O_6	−0.01	0.01	−5.02	5.02

$B_{11}O_{24}$ dipole moment in BBOF is similar to that of B_3O_6 in BBO. The dipole moments of the remaining polyhedral units in BBOF are all larger than those in BBO; however, one should be careful in making such comparisons. The crystal symmetry of BBOF ($Cmc2_1$) restricts the polar axis to be along the *c* direction; the twofold screw rotation parallel to *c* cancels the dipole contributions along the *a* and *b* axes. Examination of the dipole moments along the *c* direction (Table 1) shows that the origin of the enhanced SHG response in BBOF is hard to explain by considering the anionic groups alone, as the BBOF dipole moments are smaller than those in BBO. The cooperative action of the polyhedral dipoles requires that they be evaluated using

dx.doi.org/10.1021/ja400500m | *J. Am. Chem. Soc.* 2013, 135, 4215−4218

the complete crystal symmetry, including both point and translation operations.

Before introducing our quantitative model showing how local atomic displacements lift the inversion symmetry and allow dipole formation, we consider the role of changes in the electronic structure upon addition of F as a possible origin for the enhanced SHG response in BBOF over BBO. DFT calculations using the local density approximation (LDA) found both materials to be insulating with band gaps of ∼5 eV (Figure S8), which are lower than the experimental values (a well-known artifact of the LDA functional). As anticipated, the densities of electronic states of BBO and BBOF are very similar since there are only four F atoms in the 144 atom unit cell. The valence band (VB) largely has O 2p and B 2p character, whereas the conduction band (CB) is formed predominately by Ba 6s states strongly hybridized with O 2p orbitals. The main difference is that the F 2p states, which are centered around −2.5 eV in the VB, shift the low-energy O 2p states to higher energy because of the greater electronegativity of F relative to O. This leads to a sharp onset of well-separated electronic states in the VB just below the Fermi level. While this could lead to greater optical-transition matrix elements, such enhancements are usually negligible in wide-band-gap materials, as the energy gap separating the states participating in the transition enters into the denominator of the second-order dielectric susceptibility describing the SHG response.[16] Hence, we believe that the overall differences in the electronic structures of BBO and BBOF are not primarily responsible for the SHG enhancement; at most they provide a minimal enhancement secondary to that arising from structural differences.

To isolate the structural displacements hidden in the anionic group theory analysis that produce the acentric charge distribution, we decomposed the polar structure using an approach conceptually similar to that of Abrahams,[17] who examined how polar ferroelectrics could be designed by considering atomic displacement patterns that would drive transitions between *nonpolar* and *polar* space groups. The key is that a clear group−subgroup relationship exists. We extended this approach by applying a mode-polarization vector analysis[10] to extract quantitatively the magnitudes and directions of the polar atomic displacements contributing to the asymmetric charge density required for SHG.

We first identified a pseudosymmetric structure for BBOF with inversion symmetry in space group *Cmcm* (Figure S9 and Table S5) by performing DFT structural relaxations with the lattice constants fixed at the values in the experimental $Cmc2_1$ structure and the atomic forces restricted to be <8 meV/Å. We then examined the relationship between the *Cmcm* and $Cmc2_1$ phases in terms of orthonormal symmetry-adapted modes (i.e., irreducible representations of the high-symmetry phase compatible with the breaking of inversion symmetry in the group−subgroup pair). The two structures are related by a single polar mode with a maximum atomic displacement of 1.25 Å that splits two oxygen Wyckoff orbits (WOs): O1 and O5 in the nonpolar *Cmcm* structure split into O1/O4 and O3/O7, respectively, in $Cmc2_1$. Because the polar mode uniquely acts on each Wyckoff position (WP) of *Cmcm*, we can understand how the polar displacements arise by considering the distortions involved in each WO independently.[18] The atoms belonging to each WP and a description of the distortions are given in Table 2; the distortions are illustrated in Figures S10−S12.

Next, for each WP we computed a mode-distortion vector consisting of a normalized set of atomic displacements that, when multiplied by an amplitude $\mathcal{A}$, produces the distorted low-symmetry structure. The amplitude was computed as the square root of the sum of the squared displacements in the conventional cell: $\mathcal{A} = (\sum_{\mu,i} m(\mu, i)|\mathbf{u}(\mu, i)|^2)^{1/2}$, where $m(\mu,i)$ and $\mathbf{u}(\mu,i)$ are the multiplicity and displacement, respectively, of atom μ at atomic position i in the low-symmetry phase. Table 2 lists for each WP the value of $\mathcal{A}$ and the atom making the largest contribution in that orbit to the total amplitude (shown in bold).

Table 2. BBOF Atomic Decompositions, Distortion Types, and Total and Polar-Axis Distortion Mode Amplitudes (in Å)

WP	atom(s)[a]	distortion	$\mathcal{A}$	$\mathcal{A}_p$	$\frac{\mathcal{A}_p}{\mathcal{A}}$
4*a*	**Ba1**	displacement along *b*	1.85	0	0
4_b	**O4**	buckling of bridging O linking $B_{11}O_{24}$ chains in the *bc* plane	1.02	0.912	0.89
4*c*	**Ba2**, B3, F, O7	Ba and F displacements along *c*; B and O displacements along *c* to give a trigonal-pyramidal BO_3 unit	2.66	2.66	1
8*e*	B1, B5, **B6**, O9	buckling of B−O−B chains in the *bc* plane	3.26	1.49	0.44
8*g*	Ba3, B2, **B4**, O2, O3, O6, O8	B and O displacements along *c*	5.61	5.61	1
16*h*	O1, **O5**	O displacements to give $B1O_4$ tetrahedra	3.34	1.37	0.41

[a]The atom shown in bold for each WP makes the greatest displacement.

Our analysis indicated that some atomic displacement patterns (distinguished by WO) are more important than others in understanding the polar $Cmc2_1$ structure. The atomic displacements at WPs 4*c* and 8*g* produce the largest contributions to the total distortion of 8.17 Å, which is close to the value obtained by taking the square root of the sum of the squares of the $\mathcal{A}$ values in Table 2, indicating the linearity and orthogonality of our decomposition.[19] The 4*c* mode strictly involves displacements along the polar axis; the F distortion occurs with a correlated Ba2 displacement of 1.04 Å, increasing the Ba2−F bond length from 2.356 Å (*Cmcm*) to 2.440 Å ($Cmc2_1$). The 8*g* mode makes a greater contribution to the asymmetry in the structure (5.61 Å); it includes displacements of atoms largely within the $B_{11}O_{24}$ chains, creating tetrahedral BO_4 units through cooperative B and O distortions along the *c* axis. Ba3 is also displaced along the polar axis, filling in the tunnels created by the $B_{11}O_{24}$ units to form BaO_7 polyhedra (average Ba−O length 2.676 Å) from its nominal octahedral coordination in the *Cmcm* phase (average length 2.580 Å).

The analysis also allowed us to quantify the contribution to the asymmetric structure from atomic displacements specifically along the crystallographic axis that permit a net dipole. We projected out the vector components of the displacements for each WP and recomputed the amplitudes along the polar axis, $\mathcal{A}_p$ (Table 2). The $\mathcal{A}_p/\mathcal{A}$ ratios reveal that WPs 4*c* and 8*g* are "fully polarized", as all of the atomic displacements in those orbits contribute to lifting of the inversion symmetry and the formation of an electric dipole. Values of $\mathcal{A}_p/\mathcal{A}$ less than 1 indicate that only a fraction of the displacements within the orbit contribute to the structural asymmetry. Interestingly, displacements of Ba1 make no contribution to a local dipole (at least at the ionic level).

dx.doi.org/10.1021/ja400500m | J. Am. Chem. Soc. 2013, 135, 4215−4218

These striking structural asymmetries highlight the difficulty of applying anionic group theory approaches to materials with chain-like FBBs rather than polyhedral groups.

For comparison, we applied the same analysis to BBO (see the SI) and found $\mathcal{A}$= 5.19 Å with a small $\mathcal{A}_p$ of only 0.37 Å. Because of the different numbers of formula units per unit cell in BBO and BBOF, we defined a reduced distortion amplitude $\mathcal{A} = \mathcal{A}/\Omega$, where Ω is the conventional cell volume, to obtain specific-acentric-mode displacements (SAMDs), which provide an unbiased measure of the amounts of polar distortion per unit volume in the two crystals. We calculated SAMDs of 4.71×10^{18} and 3.10×10^{18} Å/cm^3 for BBOF and BBO, respectively, and their ratio is in remarkably good agreement with the SHG intensity ratio of 1.83, suggesting that the SAMD is an accurate descriptor of the SHG intensity. However, further studies of this type are required to evaluate the generality of the SAMD descriptor for other polar crystals.

Finally, we examined in more detail the local electronic structure, specifically focusing on Ba because of its large correlated displacements with F. The SAMD analysis does not capture the electronic effects of the Ba^{2+} cations, which were reported to be small and finite but nonzero in BBO.[7] The DFT-computed electron localization function (ELF) for BBOF (Figure 4) shows significant charge transfer from O^{2-} to Ba^{2+},

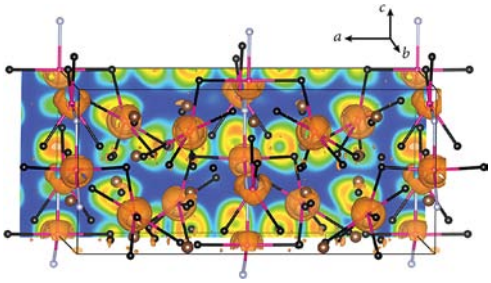

Figure 4. ELF isosurface plot for BBOF showing asymmetric charge localization (orange lobes) mainly about the Ba2 and Ba3 sites. Pink, Ba; black, O; gray, F; B has been omitted for clarity.

manifested as asymmetric lobelike isosurfaces in the ELF plot. Although the Ba 6s orbitals are spherical and form the CB, the acentric atomic distortions produce a discernible asymmetric localization of charge density about the Ba sites that contributes to the SHG intensity. In the absence of that asymmetry, Ba atoms would make no contribution.

In summary, the enhanced SHG intensity in BBOF originates mainly from F-directed polar displacements and to a lesser extent from the Ba polarizability. These features are captured within our theoretical framework integrating a crystallographic descriptor model with electronic structure calculations.

■ ASSOCIATED CONTENT

Supporting Information

Methods and additional data. This material is available free of charge via the Internet at http://pubs.acs.org.

■ AUTHOR INFORMATION

Corresponding Author

slpan@ms.xjb.ac.cn; jrondinelli@coe.drexel.edu

Notes

The authors declare no competing financial interest.

■ ACKNOWLEDGMENTS

This work was supported by the National Key Basic Research Program of China (2012CB626803), the National Natural Science Foundation of China (U1129301, 51172277, 21101168, 11104344, 21201176), the Main Direction Program of Knowledge Innovation of the Chinese Academy of Sciences (CAS) (KJCX2-EW-H03-03), the One Hundred Talents Project Foundation Program of CAS, the Major Program of Xinjiang Uygur Autonomous Region of China during the 12th Five-Year Plan Period (201130111), and the High Technology Research and Development Program of Xinjiang Uygur Autonomous Region of China (201116143). K.R.P. acknowledges support from NSF (Solid State Chemistry Award DMR-1005827); J.M.R. acknowledges support from ACS PRF (52138-DNI10).

■ REFERENCES

(1) (a) Chen, C.; Wu, Y.; Jiang, A.; Wu, B.; You, G.; Li, R.; Lin, S. *J. Opt. Soc. Am. B* **1989**, *6*, 616. (b) Wu, Y.; Sasaki, T.; Nakai, S.; Yokotani, A.; Tang, H.; Chen, C. *Appl. Phys. Lett.* **1993**, *62*, 2614. (c) Keszler, D. A.; Akella, A.; Schaffers, K. I.; Alekel, T. *MRS Proc.* **1993**, *329*, 15. (d) Wu, H.; Pan, S.; Poeppelmeier, K. R.; Li, H.; Jia, D.; Chen, Z.; Fan, X.; Yang, Y.; Rondinelli, J. M.; Luo, H. *J. Am. Chem. Soc.* **2011**, *133*, 7786. (e) Becker, P. *Adv. Mater.* **1998**, *10*, 979. (f) Pan, S.; Smit, J. P.; Watkins, B.; Marvel, M. R.; Stern, C. L.; Poeppelmeier, K. R. *J. Am. Chem. Soc.* **2006**, *128*, 11631.

(2) Wu, B.; Tang, D.; Ye, N.; Chen, C. *Opt. Mater.* **1996**, *5*, 105.

(3) (a) Halasyamani, P. S.; Poeppelmeier, K. R. *Chem. Mater.* **1998**, *10*, 2753. (b) Maggard, P. A.; Stern, C. L.; Poeppelmeier, K. R. *J. Am. Chem. Soc.* **2001**, *123*, 7742. (c) Donakowski, M. D.; Gautier, R.; Yeon, J.; Moore, D. T.; Nino, J. C.; Halasyamani, P. S.; Poeppelmeier, K. R. *J. Am. Chem. Soc.* **2012**, *134*, 7679.

(4) (a) Sun, C.-F.; Hu, C.-L.; Xu, X.; Yang, B.-P.; Mao, J.-G. *J. Am. Chem. Soc.* **2011**, *133*, 5561. (b) Zhang, J.; Zhang, Z.; Zhang, W.; Zheng, Q.; Sun, Y.; Zhang, C.; Tao, X. *Chem. Mater.* **2011**, *23*, 3752.

(5) Bera, T. K.; Jang, J. I.; Ketterson, J. B.; Kanatzidis, M. G. *J. Am. Chem. Soc.* **2009**, *131*, 75.

(6) Yu, P.; Zhou, L.-J.; Chen, L. *J. Am. Chem. Soc.* **2012**, *134*, 2227.

(7) Lin, J.; Lee, M.-H.; Liu, Z.-P.; Chen, C.; Pickard, C. J. *Phys. Rev. B* **1999**, *60*, 13380.

(8) Jerphagnon, J. *Phys. Rev. B* **1970**, *2*, 1091.

(9) (a) Chen, C.; Liu, G.-Z. *Annu. Rev. Mater. Res.* **1986**, *16*, 203. (b) Chen, C. *Sci. Sin. (Engl. Ed.)* **1979**, *22*, 756.

(10) Perez-Mato, J. M.; Orobengoa, D.; Aroyo, M. I. *Acta Crystallogr., Sect. A* **2010**, *66*, 558.

(11) (a) Huang, H.; Yao, J.; Lin, Z.; Wang, X.; He, R.; Yao, W.; Zhai, N.; Chen, C. *Angew. Chem., Int. Ed.* **2011**, *50*, 9141. (b) Yu, H.; Wu, H.; Pan, S.; Yang, Z.; Su, X.; Zhang, F. *J. Mater. Chem.* **2012**, *22*, 9665.

(12) Chen, C.; Wu, B. C.; Jiang, A. D.; You, G. M. *Sci. Sin., Ser. B (Engl. Ed.)* **1985**, *28*, 235.

(13) Kurtz, S. K.; Perry, T. T. *J. Appl. Phys.* **1968**, *39*, 3798.

(14) (a) Wang, S.; Ye, N.; Li, W.; Zhao, D. *J. Am. Chem. Soc.* **2010**, *132*, 8779. (b) Wang, S.; Ye, N. *J. Am. Chem. Soc.* **2011**, *133*, 11458.

(15) (a) Jeggo, C. R.; Boyd, G. D. *J. Appl. Phys.* **1970**, *41*, 2741. (b) Goodey, J.; Broussard, J.; Halasyamani, P. S. *Chem. Mater.* **2002**, *14*, 3174.

(16) Rashkeev, S. N.; Lambrecht, W. R. L. *Phys. Rev. B* **2001**, *63*, No. 165212.

(17) Abrahams, S. C. *Acta Crystallogr., Sect. B* **2008**, *64*, 426.

(18) Stroppa, A.; Di Sante, D.; Horiuchi, S.; Tokura, Y.; Vanderbilt, D.; Picozzi, S. *Phys. Rev. B* **2011**, *84*, 014101.

(19) The slight discrepancy is due to the arbitrariness in the choice of origin for structures without inversion symmetry. Here we chose the origin of the polar $Cmc2_1$ phase to ensure zero global translation.